# Comparison of GNSS integrated water vapor and NWM reanalysis data over Central and South America

Fernández Laura I.[1,2], Meza Amalia M.[1,2], Natali M. Paula[1,2], and Bianchi Clara E.[1,2]

[1]MAGGIA Lab. Fac. de Cs. Astronómicas y Geofísicas. Univ. Nac. de La Plata. Buenos Aires. Argentina.
[2]CONICET, Argentina.

**Correspondence:** Laura I. Fernández (lauraf@fcaglp.unlp.edu.ar)

**Abstract.** We compared and analyzed data of vertically Integrated Water Vapor (IWV) from two different re-analysis models (ERA-Interim from ECMWF and MERRA-2 from NASA's Global Modeling and Assimilation Office) with respect to IWV values from Global Navigation Satellite Systems (GNSS) at 53 stations of Central and South America during the 7-year period from January 2007 till December 2013.

5     The comparison was performed taking into account the geopotential height differences between each GNSS station and the correspondent values assigned by the models. Thus, the set of GNSS stations was divided into 3 groups: Small, Large and Critical height difference stations. Moreover, the performance of the re-analysis models was also analyzed by using an additional classification of three levels according to the mean IWV ($\overline{IWV}$) value expected at the station: $\overline{IWV} > 30 \ kg \ m^{-2}$, $12 \ kg \ m^{-2} \leqslant \overline{IWV} \leqslant 30 \ kg \ m^{-2}$ and $\overline{IWV} < 12 \ kg \ m^{-2}$.

10     Both models ($IWV_{ERA-Interim}$ and $IWV_{MERRA-2}$) offered a very good representation of the IWV from GNSS values ($IWV_{GNSS}$) for stations with a Small height difference (smaller than 100 meters). That is to say, the differences between the mean values of IWV from GNSS ($\overline{IWV}_{GNSS}$) with respect to the IWV averages from both re-analysis models are always below 7 % of the $\overline{IWV}_{GNSS}$ in the worse case.

    In general, the discrepancies between the re-analysis models with respect to $IWV_{GNSS}$ raise as the geopotential height

15 difference between the GNSS station and the static geopotential height interpolated from the models grows. Effectively, the difference between $IWV_{GNSS}$ and IWV from the re-analysis models can be as large as $10 \ kg \ m^{-2}$ for stations with a critical height difference (larger than 500 meters). For this reason, we proposed a numerical correction that compensates the effect of the geopotential height difference and the results were tested with values from ERA-Interim.

    The suggested correction was successful and reduces the differences $|IWV_{GNSS} - IWV_{ERA-Interim}|$ to less than a 7 %

20 of the mean $IWV_{GNSS}$ values. This strategy is especially recommended for stations that were classified as Critical, most of them located in mountainous areas of South America. In the case of Large height difference stations, the correction procedure is not advisable either for a coastal station and/or stations in islands. Generally in those cases, two or more grid point are on the water. Thus, the interpolated IWV value for the re-analysis model will be overestimated. At one hand, if the geopotential height of the model is smaller than the geopotential height of the GNSS station, the subtracting numerical correction would

25 compensate this overestimation of IWV near the water and thus the strategy will represent an improvement. On the other

hand, if the relationship between the geopotential heights is the opposite, the correction will be additive causing thus a worse agreement between both time series.

**Keyboards:** 3394 Instruments and techniques; 6904 Atmospheric propagation; 6964 Radio wave propagation.

## 1   Introduction

Water vapor is an abundant natural greenhouse gas of the atmosphere. The knowledge of its variability in time and space is very important to understand the global climate system (Dessler et al., 2008). Most of the regional comparisons of IWV from GNSS are aimed at validating the technique by comparing with radiosonde and radiometers where available. A complete example of this is the work of Van Malderen et al. (2014) who compared IWV GPS (Global Positioning System) with IWV derived

10   from ground-based sun photometers, radiosondes and satellite-based values from GOME, SCIAMACHY, GOME-2 and AIRS instruments at 28 sites in the northern hemisphere. Because their comparison is oriented to climatology application, they deal with long-term time series (+ 10 years). The authors asseverate that the mean biases of the GPS with the different instruments vary only between -0.3 and 0.5 $kg\ m^{-2}$ but there are large standard deviations especially for the satellite instruments.

However, some other comparisons examine the $IWV_{GNSS}$ values with respect to the respective estimates from Numerical

15   Weather Models (NWM). If focusing on the application of the current state-of-the-art reanalysis ERA-Interim from the European Centre for Medium-Range Weather Forecasts (ECMWF), both in local and global scale, some recent papers deserve to be mentioned: Heise et al. (2009) used ground pressure data from ECMWF to calculate IWV from 5-minutes Zenith Total Delay (ZTD) at stations without meteorological data available. The authors also validate their results with stations with local measurements of pressure and temperature. They also compare IWV from GPS with respect to IWV from ERA-Interim on a

20   global scale. The authors found that IWV from GPS and ECMWF show well agreement on most stations on the global scale except in mountain regions. They also addressed that temporal station pressure interpolation may result in up to 0.5 $kg\ m^{-2}$ IWV uncertainty if a local weather event happened. That is because of a misrepresentation of ECMWF analysis, especially in the tropics.

Buehler et al. (2012) compare IWV values over Kiruna in the north of Sweden from five different techniques (Radiosondes,

25   GPS, ground-based Fourier-Transform InfraRed (FTIR) spectrometer, ground-based microwave radiometer, and satellite-based microwave radiometer) with IWV from ERA-Interim reanalysis. The processed GPS dataset covers a ten-year period from November 1996 to November 2006. The authors found a good overall agreement between IWV from ERA-Interim and from GPS being the mean of differences -0.29 ± 1.02 $kg\ m^{-2}$. They also point out that ERA-Interim is drier than the GPS at small IWV values and slightly moister at high IWV values (above 15 $kg\ m^{-2}$).

30   Ning et al. (2013) evaluate IWV from GPS in comparison with IWV from ERA-Interim and IWV from the regional Rossby Centre Atmospheric (RCA) climate model at 99 European sites for a 14-year period. Because RCA is not an assimilation

model, the standard deviation of the difference RCA-GPS resulted 3 times larger than the subtraction ERA-Interim minus GPS. The IWV difference for individual sites varies from -0.21 up to 1.12 $kg\,m^{-2}$ and the corresponding standard deviation is 0.35 $kg\,m^{-2}$. In this work, the authors also highlight that the models overestimate IWV for sites near the sea.

Bordi et al. (2014) studied global trend patterns of a yearly mean of IWV from ERA-20CM and ERA-Interim. The authors highlight a regional dipole pattern of inter-annual climate variability over South America from ERA-Interim data. According to this study, the Andean Amazon basin and Northeast Brazil are characterized by rising and decreasing water content associated with water vapor convergence (divergence) and upward (downward) mass fluxes, respectively. Besides, the authors also compared IWV from ERA-Interim with the values estimated at 2 GPS stations in Bogotá and Brasilia. Such comparison on monthly timescale made known a systematic bias attributed to a lack of coincidence in the elevation of the GPS stations and the model grid points.

Tsidu et al. (2015) presented a comparison between IWV from a Fourier Transform InfraRed spectrometer (FTIR, at Addis Ababa), GPS, radiosondes, and ERA-Interim over Ethiopia for the period 2007-2011. The study is focused on the characterization of the different error sources affecting the data time series. In particular, from the study of diurnal and seasonal variabilities, the authors addressed differences in the magnitude and sign of IWV bias between ERA-Interim and GPS. They linked this effect with the sensitivity of the convection model with respect to the topography.

Wang et al. (2015) performed a 12-year comparison of IWV from 3 third generation atmospheric reanalysis models including ERA-Interim, MERRA and the Climate Forecast System Reanalysis (CFSR) on a global scale. IWV values from the reanalysis models were also compared with radiosonde observations in land and Remote Sensing Systems (RSS) on satellites over oceans. The authors asseverate that the main discrepancies of the 3 datasets among them are in Central Africa, Northern South America, and highlands.

In this paper, we investigate the differences between $IWV_{GNSS}$ resulted from a geodetic process of (GPS + GLONASS) data collected during more than 5 years in South America (Bianchi et al., 2016a) and IWV values given by ERA-Interim and MERRA-2. The comparison was performed taking into account the geopotential height differences ($\Delta Z$) between each GNSS station and the correspondent height values assigned by the models. Provided that both models showed a very good representation of the IWV values for stations with a Small height difference, we used this set of stations with $\Delta Z$ smaller than 100 meters, to deeply analyze the expected seasonal behavior according to the inter-annual mean of IWV from GNSS expected at the station. In order to take into account the differences found in IWV values from the models at stations with $\Delta Z$ larger than 100 m., we proposed a numerical correction. The strategy was tested for ERA-Interim re-analysis model and it shows to be successful. Section 2 describes the different sets of data used in this study. Follows the explanation of the methodology and the presentation of the results obtained after applying the proposed correction to IWV values from ERA-Interim.

## 2 Data

### 2.1 IWV from GNSS

In this study, the GNSS data is the main source of information for the spatial and temporal distribution of water vapor. Thus, the main variable considered is the IWV estimated from the delay caused by the troposphere to the GNSS radio signals during

5  its travel from the satellite to the ground receiver. The total delay projected onto the zenith direction (ZTD) is usually split into two contributions: the hydrostatic delay (ZHD, Zenith Hydrostatic Delay) depending merely on the atmospheric pressure and the Zenith Wet Delay (ZWD) depending mainly on the humidity. Finally, $IWV_{GNSS}$ can be obtained from ZWD multiplying it by a function of the mean temperature of the atmosphere.

The reference database of $IWV_{GNSS}$ (GPS + GLONASS) used in this study come from a geodetic process over 136 tracking

10  stations in the American Continent placed from southern California to Antarctica, during the 7-year period from January 2007 till December 2013 (Bianchi et al., 2016b). Specifically, the data series of $IWV_{GNSS}$ used in this study is restricted to those 69 stations with IWV time series spanning more than 5 years.

The GNSS observations were processing at a double-difference level with the Bernese GNSS Software 5.2 (Dach et al., 2015) where all the models and conventions employed are recommended by the International Earth Rotation and Reference

15  Systems Service (IERS). The geodetic process used Vienna Mapping Function 1 (VMF1) (Boehm et al., 2006). The ZTD were represented as 30-minutes linear piecewise estimates and compared with three solutions contributing to the International GNSS Service (IGS) for the repro2 reanalysis. The comparison of ZTD results shows the expected consistency between estimations from the homogeneous but independent analysis. Afterward, to achieve $IWV_{GNSS}$ estimations, it is necessary to subtract the modeled ZHD from the ZTD data in order to obtain ZWD. ZHD are computed following Davis et al. (1985) and considering

20  observed pressure measurements from nearby GNSS stations. Finally, the $IWV_{GNSS}$ values every 30 minutes are obtained from ZWD by using the proportionality constant from Askne and Nordius (1987). More details of the ZTD geodetic processing and the steps to obtain the IWV values are at Bianchi et al. (2016a).

### 2.1.1 IWV from NWM

The values of columnar Integrated content of Water Vapor (IWV) as reanalysis products from ERA-Interim (Dee et al., 2011)

25  and MERRA-2 (Gelaro et al., 2017; Bosilovich et al., 2015) were evaluated in this study. The horizontal resolutions are $0.25° \times 0.25°$ for ERA-Interim and $0.625° \times 0.50°$ for MERRA-2, respectively. Because ERA-Interim data is given 4 times a day, in order to perform the comparison and even if MERRA-2 gives hourly data, we pick up IWV data from MERRA-2 every 6 hours at 0, 6, 12 and 18 hours of Universal Time.

ERA-Interim is the global atmospheric reanalysis produced by the European Centre for Medium-Range Weather Forecasts

30  (ECMWF). It covers the period from 1979 up today and supersedes the ERA-40 reanalysis. ERA-Interim address some difficulties of ERA-40 in data assimilation mainly related to the representation of the hydrological cycle, the quality of the stratospheric circulation, and the consistency in time of reanalyzed geophysical fields (Dee et al., 2011).

MERRA-2 is the successor of The Modern-Era Retrospective Analysis for Research and Applications (MERRA) from NASA's Global Modeling and Assimilation Office (Rienecker et al., 2011). MERRA-2 represents a quality improvement compared with MERRA because of the trends and jumps linked to changes in the observing systems. Additionally, MERRA-2 assimilates observations not available to MERRA and reduces bias and imbalances in the water cycle (Gelaro et al., 2017).

5 Moreover, the longitudinal resolution of MERRA-2 data is changed from $0.667°$ in MERRA to $0.625°$ whereas the latitudinal resolution remains unchanged ($0.5°$) (Bosilovich et al., 2015).

To this application we used the gridded values of the vertical Integral of Water Vapor (IWV) from both re-analysis models. Because the comparison is performed at each GNSS station, a bilinear interpolation of each gridded data set was performed. In addition, we use values of air temperature ($T$) and specific humidity ($q$) from ERA-Interim for the calculation of the correction

10 to the IWV values. Both, $q$ and $T$, are given in 37 levels of atmospheric pressure from 1000 to 1 hPa.

## 3 Methodology:

### 3.1 Stations classification criteria

Even when both reanalysis model give gridded values of the vertical integral of the water vapor, the solution provided by each model is linked to its respective geopotential surface invariant. Usually, IWV values are interpolated from the original grid

15 by applying bilinear interpolation. Nevertheless, elevation differences between geopotential height from each model grid and GNSS height must be addressed. Effectively, if the height of a given point from a model is located lower than the position of the receiver, the model integrates a larger column of water vapor and the opposite if the model locates upper than it.

We performed the present comparison establishing a selection criterion according to the difference of geopotential height ($Z$) between each reanalysis model and the GNSS height at the station. In order to compute the geopotential height of the

20 GNSS stations ($Z_{GNSS}$) we followed Van Dam et al. (2010) algorithm. First we obtained the orthometric height at each GNSS station by correcting the ellipsoidal height with the EGM08 model (Pavlis et al., 2012). For a given GNSS station, the respective geopotential height from each of the 2 reanalysis models resulted from a bilinear interpolation of each respective gridded dataset.

Thus, if $\Delta Z$ refers to the difference between $Z_{GNSS}$ and $Z_{NWM}$ (see Figure 1),

25
$$|\Delta Z| = |Z_{GNSS} - Z_{NWM}| \tag{1}$$

where NWM corresponds to ERA-Interim or MERRA-2. We classified the whole set of stations in 3 categories: a) Small height difference ($|\Delta Z| < 100m.$) b) Large height difference ($100m. \leq |\Delta Z| \leq 500m.$) and c) Critical height difference ($|\Delta Z| > 500m.$).

Table 1 shows the geodetic coordinates as well as the climate classification of Köppen-Geiger (K-G) (Peel et al., 2007)

30 and the $|\Delta Z|$ classification for both models. Subsequently, we selected the common stations that address the adopted criteria simultaneously in both NWM. Thus the original set of 69 stations is reduced to 53 stations. Figure 2 shows the 53 GNSS stations arrangement according to $|\Delta Z|$ differences with respect to ERA-Interim.

## 3.2 Computation of the integral correction

Once we detected the cases in which the application of a correction is necessary, we proceed to describe the proposed integral correction. It will be calculated only for one of the two tested re-analysis models.

Zhu (2014) compare the results of several reanalysis projects with independent sounding observations recorded in the Eastern Himalayas during June 2010. Among all the reanalysis models, ERA-Interim and MERRA were included. The authors analyze temperature, specific humidity, u-wind, and v-wind between 100 hPa and 650 hPa. They found that ERA-Interim showed the best performance for all variables including specific humidity the key variable to produce the integrated water vapor. Even if we tested MERRA-2, which is an improvement of MERRA, ERA-Interim is having a smaller grid. Thus, following Zhu (2014) criteria and taking advantage of a thinner grid, we used air temperature ($T$) and specific humidity ($q$) on 37 pressure levels from ERA-Interim data to test the proposed correction. Following we describe how this correction is computed.

The starting data are the GNSS geopotential height ($Z_{GNSS}$) that is set as a reference, and the value of the geopotential height from ERA-Interim ($Z_{model}$) obtained after a bi-linear interpolation. According to our classification, these two values are not the same but may differ several hundred meters. Because the geodetic coordinates ($\phi$, $\lambda$, $h$) of the GNSS station are known, we can compute the respective geopotential height as (Van Dam et al., 2010)

$$Z_{GNSS} = \frac{g_s(\phi)\, C(\phi)\, h}{g_0\, (C(\phi) + h)} \qquad (2)$$

where $g_0 = 9.80665\, m\, s^{-2}$ is the normal gravity at $45°$ latitudes, the ellipsoidal height ($h$) is referred to the ellipsoid WGS84 and thus the radius of the ellipsoid at geodetic latitude $\phi$ is,

$$C(\phi) = \left( \frac{cos^2(\phi)}{a^2} + \frac{sin^2(\phi)}{b^2} \right)^{-1/2} \qquad (3)$$

with $a = 6378137 m.$ and $b = 6356752.3142 m.$ are the semimajor and semiminor axis of the WGS84 ellipsoid, respectively (Hofmann-Wellenhof and Moritz, 2006). Moreover, the value of the gravity on the ellipsoid at geodetic latitude $\phi$ can be written as (Van Dam et al., 2010).

$$g_s(\phi) = g_E \frac{1 + k_s\, sin^2(\phi)}{\sqrt{1 - e^2\, sin^2(\phi)}} \qquad (4)$$

with $e^2 = 0.00669437999014$ is the first eccentricity squared of the WGS84 ellipsoid and $g_E = 9.7803253359 m\, s^{-2}$ is the normal gravity at the Equator (Hofmann-Wellenhof and Moritz, 2006) and $k_s = 0.001931853$ (Van Dam et al., 2010).

Afterward, the expression of the pressure at the geopotential height ($Z$) with respect to a given reference level is (Van Dam et al., 2010)

$$p(Z) = p_0 \left( \frac{T_0 - \lambda\, \delta Z}{T_0} \right)^{g_0/R\lambda} \qquad (5)$$

where $T_0$ and $p_0$ refer to the temperature and pressure values at a reference level, $R = 287.04\, J\, kg^{-1}\, °K$ is the gas constant and $\lambda = 0.006499\, °K\, m^{-1}$ is the lapse rate of the temperature, and $\delta Z$ is the geopotential height difference between $Z$ and the reference level.

Accordingly, given a $Z_{GNSS}$ at each instant, we have to look for the immediate upper geopotential height level from ERA Interim among the 37 available levels. We should consider that at any time the pressure value of each level is constant but it does not necessarily happen the same with the geopotential height.

Let suppose that this level is 27 that corresponds to 750 hPa. Figure 3 illustrates the example. The value of IWV provided by ERA-Interim is the result of the numerical integration of the expression (Berrisford et al., 2011).

$$IWV_{ERA-Interim} = \frac{1}{g_0} \int_{p_1}^{p_s} q(p)\, dp \tag{6}$$

where $g_0$ is the standard acceleration of the gravity at mean sea level, $q(p)$ is the specific humidity of the air at the pressure level $p$ and the integral is calculated from the first level ($p_1$) up to the model surface level ($p_s$), i.e. up to the static geopotential height ($Z_{model}$) that corresponds to the station.

Therefore, by using temperature and specific humidity values given at the 2 layers above and below the point of interest, we have to interpolate $T$ and $q$ at the GNSS geopotential level ($Z_{GNSS}$). Because the pressure value at $Z_{model}$ is not necessarily coincident with one of the given levels, we could also extrapolate $T$ and $q$ in the same way for $Z_{model}$.

Finally, the $\Delta IWV$ is computed as the numerical integral of Eq. (6) between the pressure values at $Z_{model}$ and at $Z_{GNSS}$. This quantity could be additive if $Z_{GNSS} < Z_{model}$ or subtractive if opposite.

# 4  Results

The Table 2 shows the inter-annual IWV mean values for the 53 stations of the reduced subset that fulfill the station´s selection criteria by using the $|\Delta Z|$, i.e. ($Z_{GNSS} - Z_{NWM}$). IWV inter-annual averages were computed for GNSS ($\overline{IWV}_{GNSS}$) as well as for both NWM ($\overline{IWV}_{ERA-Interim}$ and $\overline{IWV}_{MERRA-2}$) . Note that MERRA-2 values could be a little more dispersive because of the coarser grid. However, the correlation coefficients between $\overline{IWV}_{GNSS}$ values and the respective ones for both NWM, are higher than 0.95 in most of the cases.

## 4.1  Analysis of the efficiency of the re-analysis models

In order to analyze the performance of ERA-Interim and MERRA-2, we compared both mean inter-annual averages of IWV ($\overline{IWV}_{ERA-Interim}$ and $\overline{IWV}_{MERRA-2}$) with respect to $\overline{IWV}_{GNSS}$.

Regarding Table 2 for Small $|\Delta Z|$ stations, and focusing on ERA-Interim, the subtractions of $\overline{IWV}_{GNSS}$ minus $\overline{IWV}_{ERA-Interim}$ have different signs but they are smaller than 3 $kg\,m^{-2}$ but RNNA station where it reaches 3.5 $kg\,m^{-2}$. On the other hand, the differences between ($\overline{IWV}_{GNSS} - \overline{IWV}_{MERRA-2}$) never surpass 3.5 $kg\,m^{-2}$. Moreover, generally $\overline{IWV}_{MERRA-2}$ resulted larger than $\overline{IWV}_{GNSS}$ and that overestimation of MERRA-2 can be seen despite the sign of $|\Delta Z|$.

In general for stations classified as Small, IWV mean values from ERA-Interim are closer to mean values from GNSS than MERRA-2. Moreover, the $\overline{IWV}_{NWM}$ disagreement from GNSS values is about a 7 % of $\overline{IWV}_{GNSS}$ for stations with $\overline{IWV} > 30 \; kg\,m^{-2}$ and it remains in 7 % for stations with $12 \; kg\,m^{-2} \leqslant \overline{IWV} \leqslant 30 \; kg\,m^{-2}$. Furthermore, there is only one

station that fulfill the condition $\overline{IWV} < 12\ kg\ m^{-2}$ and its maximum discrepancy is with MERRA-2 reaching $\backsim 6\%$ of the $\overline{IWV}_{GNSS}$.

Among Large $|\Delta Z|$ stations the situation also depends on the $\overline{IWV}$ expected. Thus, when $\overline{IWV} > 30\ kg\ m^{-2}$ the disagreement of MERRA-2 reaches $\backsim 15\%$ of $\overline{IWV}_{GNSS}$ while for ERA-Interim it is about 9 %. In the case of stations that fulfill the condition $12\ kg\ m^{-2} \leqslant \overline{IWV} \leqslant 30\ kg\ m^{-2}$, the discrepancies could reach up to $\backsim 35$ % and for stations with $\overline{IWV} < 12\ kg\ m^{-2}$ the disagreement of both models with respect to $\overline{IWV}_{GNSS}$ is below 40 % of this amount. For Critical $|\Delta Z|$ stations the discrepancies of the NWM with respect to GNSS can reach $\backsim 55\%$ of the $\overline{IWV}_{GNSS}$.

In general, we can observe that the percentages of model failures grow as the height differences ($\Delta Z$) become larger. All of the above, we asseverate that the disagreement is the greatest for the stations classified as Critical.

Thus, provided that both models showed a very good representation of the IWV values for stations with a Small height difference, we will focus on such stations to analyze the seasonal behavior of each NWM with respect to $IWV_{GNSS}$. The objective is to distinguish a systematic lack of agreement between NWM and GNSS, if there are any.

Figure 4 shows the seasonal stacked $\Delta IWV$ for both models. Three cases among the Small height difference stations are shown as an example for $\overline{IWV} > 30\ kg\ m^{-2}$ (BELE), $12\ kg\ m^{-2} \leqslant \overline{IWV} \leqslant 30\ kg\ m^{-2}$ (LPGS) and $\overline{IWV} < 12\ kg\ m^{-2}$ (FALK). At BELE the differences from MERRA2 are always larger than the ones from ERA-Interim. Such differences also have a different sign indicating that ERA-Interim always underestimates $\overline{IWV}_{GNSS}$ but it hardly exceeds $3\ kg\ m^{-2}$, while MERRA2 always overestimate $\overline{IWV}_{GNSS}$ and the disagreement could reach $3.5\ kg\ m^{-2}$. For LPGS both NMW overestimate within $1\ kg\ m^{-2}$. Finally at FALK station both re-analysis models overestimate the inter-annual seasonal mean of IWV from GNSS although MERRA-2 values are always larger than ERA-Interim ones. As we said before, even though such a difference never exceed $1\ kg\ m^{-2}$, that represents about 10 % of the total amount because $\overline{IWV} < 12\ kg\ m^{-2}$.

### 4.2  Application of the integral correction

From the analysis of the behavior of the Small height difference stations, we can see that both NWM represent IWV from GNSS better than a 7% of the expected values in the worse case. Thus, we propose to compute a correction to the IWV values from ERA Interim only for stations classified as Large and Critical. Such a compensation have to be added (or subtracted) to the given $IWV_{ERA-Interim}$ values considering the sign of the height differences. Accordingly, the proposed correction will be calculated as the numerical integration of the specific humidity ($q$) between the geopotential height from ERA-Interim and the geopotential height of the GNSS station (see Section 3.2).

Figure 5 shows the application of the before mentioned correction procedure on two Critical height difference stations: BOGT in Bogotá, Colombia, and SANT in Santiago de Chile, Chile. These stations are selected because their $\Delta Z$ is having a different sign. As expected both curves $IWV_{GNSS}$ (blue solid line) and $IWV_{ERA-Interim}$ (green solid line) are not coincident. In the case of BOGT, $\Delta Z$ is positive, that means that GNSS station is higher to the location assigned by ERA-Interim. Accordingly, the model integrates a thicker layer of atmosphere and thus $IWV_{ERA-Interim}$ values resulted larger than ones from $IWV_{GNSS}$. The opposite can be seen in SANT. Figure 5 also shows us an improvement of the agreement with respect to $IWV_{GNSS}$ when we add the correction to the values of the $IWV_{ERA-Interim}$ (red dashed line).

Figure 6 shows the residuals with and without applying the integral correction. We can see that the differences ($IWV_{GNSS} -$ $IWV_{ERA-Interim}$), which can reach up to 10 $kg\,m^{-2}$, are reduced to an order of magnitude of their respective value of $\overline{IWV}_{GNSS}$ (solid black line).

However, the application of this correction in the case of stations classified as Large should be more precautionary. This
5    set of stations showed a heterogeneous behavior and include some cases where the application of the correction not only is unnecessary, but it can make the differences ($IWV_{GNSS} - IWV_{ERA-Interim}$) even larger. Effectively, in these cases different shortcomings of the model overlap the height problem and therefore the proposed correction does not work. As an example of this we can mention the case of coastal and/or insular stations where 2 or more grid points will be in the ocean. In all these cases the value of IWV calculated from the bilinear interpolation will be overvalued. Let's analyze in detail the case of stations near
10    the seashore (for example PARC in Punta Arenas, Chile) where 2 of the 4 grid points are in the ocean (see Figure 7). Also $\Delta Z$ = -117.12 m in PARC indicating that the geopotential height from ERA-Interim is larger than the GNSS geopotential height and therefore the proposed correction will be additive. Besides this result, the $IWV_{ERA-Interim}$ resulted over-estimated by applying a bilinear interpolation that uses data points in the ocean. In conclusion, the value ($IWV_{ERA-Interim} + correction$) will result larger than the $IWV_{GNSS}$ value that you intend to estimate. Thus, this is an example where applying the suggested
15    correction may worsen the results.

## 5    Discussion and Conclusions

In this work, we analyzed the discrepancies between the vertically Integrated Water Vapor values provided by two re-analysis models (ERA-Interim and MERRA-2) with respect to the $IWV_{GNSS}$ values taken as a reference in the South and Central American continent. We performed the comparison establishing a selection criteria according to the difference of static geopo-
20    tential height ($\Delta Z$) between GNSS and each reanalysis model at the station.

Several authors had been reported problems related to the elevation correction for data from the reanalysis models. The artificial bias in IWV introduced by this altitude difference was previously reported by Bock et al. (2007);Van Malderen et al. (2014);Bordi et al. (2014) and Bianchi et al. (2016a). Moreover, this effect can also affect other variables. For instance, Gao et al. (2012) studied the height corrections for the ERA-Interim 2m-temperature data at the Central Alps and they also found
25    large biases that must be corrected in mountainous areas.

For the above, an integral correction was proposed that compensates the effect of the geopotential height difference between GNSS and the interpolated grid point in the reanalysis model and the results were tested with the respective ones from ERA-Interim. The correction is computed as the numerical integration of the specific humidity where the integral limit is a pressure difference at $\delta Z$ (see Eqs. 5 and 6 ).
30    Before computing the correction, the set of GNSS stations was divided into 3 groups according to the differences $\Delta Z$: Small height stations ($|\Delta Z| < 100m.$), Large height stations ($100m. \leq |\Delta Z| \leq 500m.$) and Critical height stations($|\Delta Z| > 500m.$).

For the Small height stations MERRA-2 mostly exhibits the larger discrepancies, i.e. $\left|\overline{IWV}_{GNSS} - \overline{IWV}_{MERRA-2}\right| >$ $\left|\overline{IWV}_{GNSS} - \overline{IWV}_{ERA-Interim}\right|$, and this could be a consequence of a coarser horizontal grid used to the bilinear interpolation of data. Moreover, MERRA-2 generally overestimates $IWV_{GNSS}$ because $IWV_{MERRA-2} > IWV_{ERA-Interim}$.

Both for Small and Large $|\Delta Z|$ stations the discrepancies between the NWM and GNSS can be analyzed depending on the $\overline{IWV}$ expected, but anyway the differences rise as the $|\Delta Z|$ grows. For $\overline{IWV} > 30 \ kg \ m^{-2}$ the disagreement of the NWM with respect to GNSS is $\smile$ 7% for Small $|\Delta Z|$ stations but it rise up to 15 % of $\overline{IWV}_{GNSS}$ for Large stations. If $12 \ kg \ m^{-2} \leqslant \overline{IWV} \leqslant 30 \ kg \ m^{-2}$, the disagreement of the NWM goes from $\smile$ 7% for stations classified as Small up to $\smile$ 35% for Large $|\Delta Z|$ stations. Finally, for $\overline{IWV} < 12 \ kg \ m^{-2}$ the percentage of disagreement is always lower than 40 % of $\overline{IWV}_{GNSS}$ in the worse case,i.e. for Large $|\Delta Z|$ stations.

For Critical $|\Delta Z|$ stations the discrepancies of the IWV from NWM with respect to IWV from GNSS can reach $\smile$ 55% of the expected values.

All of the above, we proposed the numerical correction only for the Large and Critical stations. The suggested improvement was successful reducing the differences between $IWV_{GNSS}$ and $IWV_{ERA-Interim}$ from typical values of $10 \ kg \ m^{-2}$ to an order of magnitude of their respective value of $\overline{IWV}_{GNSS}$. The correction is especially recommended for stations that were classified as Critical, most of them located in mountainous areas of South America.

*Author contributions.* L.I. Fernández led the study and contributed to data collection, analysis, and interpretation of the results; A.M. Meza and M.P. Natali co-wrote the paper. They also contributed to the statistical analysis and the interpretation of the results. C. E. Bianchi contributed to data collection. All authors read and approved the final manuscript.

*Competing interests.* The authors declare that they have no conflict of interest.

*Acknowledgements.* This research was supported by the National Scientific and Technical Council of Argentina (CONICET) PIP 112-201201-00292 and La Plata National University (UNLP) project 11G/142. We would also like to thank the people, organizations and agencies responsible to collect, compute, maintain and openly provide the observations and the products employed in this work: The European Centre for Medium-Range Weather Forecasts (ECMWF) for providing the ERA-Interim reanalysis data (http://apps.ecmwf.int/datasets/). and the Global Modeling and Assimilation Office (GMAO) from National Aeronautics and Space Administration (NASA, USA) for providing MERRA-2 data (https://gmao.gsfc.nasa.gov/reanalysis/MERRA-2/).

# References

Askne, J. and Nordius, H.: Estimation of tropospheric delay for microwaves from surface weather data, Radio Science, 22, 379–386, https://doi.org/10.1029/rs022i003p00379, 1987.

Berrisford, P., Kållberg, P., Kobayashi, S., Dee, D., Uppala, S., Simmons, A. J., Poli, P., and Sato, H.: Atmospheric conservation properties
in ERA-Interim, Quarterly Journal of the Royal Meteorological Society, 137, 1381–1399, https://doi.org/10.1002/qj.864, 2011.

Bianchi, C. E., Mendoza, L. P. O., Fernández, L. I., Natali, M. P., Meza, A. M., and Moirano, J. F.: Multi-year GNSS monitoring of
atmospheric IWV over Central and South America for climate studies, Annales Geophysicae, 34, 623–639, https://doi.org/10.5194/angeo-34-623-2016, 2016a.

Bianchi, C. E., Mendoza, L. P. O., Fernández, L., Natali, M. P., Meza, A., and Moirano, J.: Time series of atmospheric water vapour and
troposphere zenith total delay, over Central and South America, from a homogeneous GNSS reprocessing (MAGGIA ZTD & IWV Solu-
tion 1), https://doi.org/10.1594/PANGAEA.858234, https://doi.org/10.1594/PANGAEA.858234, supplement to: Bianchi, C et al. (2016):
Multi-year GNSS monitoring of atmospheric IWV over Central and South America for climate studies. Annales Geophysicae, 34(7),
623-639, https://doi.org/10.5194/angeo-34-623-2016, 2016b.

Bock, O., Bouin, M.-N., Walpersdorf, A., Lafore, J. P., Janicot, S., Guichard, F., and Agusti-Panareda, A.: Comparison of ground-based
GPS precipitable water vapour to independent observations and NWP model reanalyses over Africa, Quarterly Journal of the Royal
Meteorological Society, 133, 2011–2027, https://doi.org/10.1002/qj.185, 2007.

Boehm, J., Niell, A., Tregoning, P., and Schuh, H.: Global Mapping Function (GMF): A new empirical mapping function based on numerical
weather model data, Geophysical Research Letters, 33, https://doi.org/10.1029/2005gl025546, 2006.

Bordi, I., Bonis, R. D., Fraedrich, K., and Sutera, A.: Interannual variability patterns of the world's total column water content: Amazon
River basin, Theoretical and Applied Climatology, 122, 441–455, https://doi.org/10.1007/s00704-014-1304-y, 2014.

Bosilovich, M. G., Lucchesi, R., and Suarez, M.: MERRA-2: File Specification, https://ntrs.nasa.gov/search.jsp?R=20150019760, 2015.

Buehler, S. A., Östman, S., Melsheimer, C., Holl, G., Eliasson, S., John, V. O., Blumenstock, T., Hase, F., Elgered, G., Raffalski, U., Nasuno,
T., Satoh, M., Milz, M., and Mendrok, J.: A multi-instrument comparison of integrated water vapour measurements at a high latitude site,
Atmospheric Chemistry and Physics, 12, 10 925–10 943, https://doi.org/10.5194/acp-12-10925-2012, https://www.atmos-chem-phys.net/
12/10925/2012/, 2012.

Dee, D. P., Uppala, S. M., Simmons, A. J., Berrisford, P., Poli, P., Kobayashi, S., Andrae, U., Balmaseda, M. A., Balsamo, G., Bauer, P.,
Bechtold, P., Beljaars, A. C. M., van de Berg, L., Bidlot, J., Bormann, N., Delsol, C., Dragani, R., Fuentes, M., Geer, A. J., Haimberger,
L., Healy, S. B., Hersbach, H., Hólm, E. V., Isaksen, L., Kållberg, P., Köhler, M., Matricardi, M., McNally, A. P., Monge-Sanz, B. M.,
Morcrette, J.-J., Park, B.-K., Peubey, C., de Rosnay, P., Tavolato, C., and Thépaut, J.-N.; Vitart, F.: The ERA-Interim reanalysis: configu-
ration and performance of the data assimilation system, Quarterly Journal of the Royal Meteorological Society, 137, issue 656, 553–597,
https://doi.org/10.1002/qj.828, 2011.

Dessler, A. E., Zhang, Z., and Yang, P.: Water-vapor climate feedback inferred from climate fluctuations, 2003–2008, Geophysical Research
Letters, 35, https://doi.org/10.1029/2008gl035333, 2008.

Gao, L., Bernhardt, M., and Schulz, K.: Elevation correction of ERA-Interim temperature data in complex terrain, Hydrology and Earth Sys-
tem Sciences, 16, 4661–4673, https://doi.org/10.5194/hess-16-4661-2012, https://www.hydrol-earth-syst-sci.net/16/4661/2012/, 2012.

Gelaro, R., McCarty, W., Suárez, M. J., Todling, R., Molod, A., Takacs, L., Randles, C. A., Darmenov, A., Bosilovich, M. G., Reichle, R., et al.: The modern-era retrospective analysis for research and applications, version 2 (MERRA-2), Journal of Climate, 30, 5419–5454, 2017.

Heise, S., Dick, G., Gendt, G., Schmidt, T., and Wickert, J.: Integrated water vapor from IGS ground-based GPS observations: initial results
5    from a global 5-min data set, Annales Geophysicae, 27, 2851–2859, https://doi.org/10.5194/angeo-27-2851-2009, 2009.

Hofmann-Wellenhof, B. and Moritz, H.: Physical geodesy, Springer Science & Business Media, 2006.

Ning, T., Elgered, G., Willén, U., and Johansson, J. M.: Evaluation of the atmospheric water vapor content in a regional climate model using ground-based GPS measurements, Journal of Geophysical Research: Atmospheres, 118, 329–339, https://doi.org/10.1029/2012jd018053, 2013.

10 Pavlis, N. K., Holmes, S. A., Kenyon, S. C., and Factor, J. K.: The development and evaluation of the Earth Gravitational Model 2008 (EGM2008), Journal of geophysical research: solid earth, 117, 2012.

Peel, M. C., Finlayson, B. L., and Mcmahon, T. A.: Updated world map of the Köppen-Geiger climate classification, Hydrology and Earth System Sciences, 11, 1633–1644, https://doi.org/10.5194/hess-11-1633-2007, 2007.

Rienecker, M. M., Suarez, M. J., Gelaro, R., Todling, R., Bacmeister, J., Liu, E., Bosilovich, M. G., Schubert, S. D., Takacs, L., Kim, G.-K.,
15    and et al.: MERRA: NASA's Modern-Era Retrospective Analysis for Research and Applications, Journal of Climate, 24, 3624–3648, https://doi.org/10.1175/jcli-d-11-00015.1, 2011.

Tsidu, G. M., Blumenstock, T., and Hase, F.: Observations of precipitable water vapour over complex topography of Ethiopia from ground-based GPS, FTIR, radiosonde and ERA-Interim reanalysis, Atmospheric Measurement Techniques, 8, 3277–3295, https://doi.org/10.5194/amt-8-3277-2015, 2015.

20 Van Dam, T., Altamimi, Z., Collilieux, X., and Ray, J.: Topographically induced height errors in predicted atmospheric loading effects, Journal of Geophysical Research, 115, https://doi.org/10.1029/2009jb006810, 2010.

Van Malderen, R., Brenot, H., Pottiaux, E., Beirle, S., Hermans, C., Mazière, M. D., Wagner, T., Backer, H. D., and Bruyninx, C.: A multi-site intercomparison of integrated water vapour observations for climate change analysis, Atmospheric Measurement Techniques, 7, 2487–2512, https://doi.org/10.5194/amt-7-2487-2014, 2014.

25 Wang, Y., Zhang, Y., Fu, Y., Li, R., and Yang, Y.: A climatological comparison of column-integrated water vapor for the third-generation reanalysis datasets, Science China Earth Sciences, 59, 296–306, https://doi.org/10.1007/s11430-015-5183-6, 2015.

Zhu, J.-H., S.-P. M. H. Z. L. Z. L. P.: Evaluation of reanalysis products with in situ GPS sounding observations in the Eastern Himalayas, Atmos. Oceanic Sci. Lett., 7, 17–22, https://doi.org/10.3878/j.issn.1674-2834.13.0050, 2014.

Table 1: GNSS stations classified by $|\Delta Z|$

| GNSS station | Geodetic coordinates | | | Classification | | |
| | Longitude [°] | Latitude [°] | Height [m] | K-G | ERA-Interim | MERRA-2 |
|---|---|---|---|---|---|---|
| BELE | -48.4626 | -1.4088 | 9.1 | Af | Small | Small |
| BYSP | -66.1612 | 18.4078 | 49.2 | Af | Small | Large |
| CUCU | -72.4879 | 7.8985 | 311.2 | Af | Critical | Critical |
| RIOB | -67.8028 | -9.9655 | 172.6 | Af | Small | Small |
| SAVO | -38.4323 | -12.9392 | 76.3 | Af | Small | Small |
| SSA1 | -38.5165 | -12.9752 | -2.1 | Af | Small | Large |
| MAPA | -51.0973 | 0.0467 | -4.2 | Am | Small | Small |
| ONRJ | -43.2243 | -22.8957 | 35.6 | Am | Large | Large |
| POVE | -63.8963 | -8.7093 | 119.6 | Am | Small | Small |
| RIOD | -43.3063 | -22.8178 | 8.6 | Am | Large | Large |
| RECF | -34.9515 | -8.0510 | 20.1 | As | Large | Small |
| RNNA | -35.2077 | -5.8361 | 45.9 | As | Small | Small |
| ACYA | -99.9030 | 16.8380 | -4.9 | Aw | Large | Large |
| BOAV | -60.7011 | 2.8452 | 69.5 | Aw | Small | Small |
| BRFT | -38.4255 | -3.8774 | 21.7 | Aw | Small | Large |
| CEEU | -38.4255 | -3.8775 | 21.7 | Aw | Small | Large |
| CEFE | -40.3195 | -20.3108 | 14.3 | Aw | Large | Large |
| CHET | -88.2992 | 18.4953 | 3.0 | Aw | Small | Small |
| CRO1 | -64.5843 | 17.7569 | -32.0 | Aw | Small | Small |
| CUIB | -56.0699 | -15.5553 | 237.5 | Aw | Small | Large |
| MABA | -49.1223 | -5.3624 | 79.8 | Aw | Small | Large |
| MANA | -86.2490 | 12.1489 | 71.0 | Aw | Large | Large |
| MSCG | -54.5407 | -20.4409 | 676.5 | Aw | Large | Large |
| PBCG | -35.9071 | -7.2137 | 534.1 | Aw | Large | Large |
| SALU | -44.2125 | -2.5935 | 19.0 | Aw | Small | Small |
| SCUB | -75.7623 | 20.0121 | 20.9 | Aw | Large | Large |
| SSIA | -89.1166 | 13.6971 | 626.6 | Aw | Large | Large |
| TAMP | -97.8640 | 22.2783 | 21.0 | Aw | Small | Small |
| TOPL | -48.3307 | -10.1711 | 256.5 | Aw | Small | Large |
| VITH | -64.9692 | 18.3433 | 4.4 | Aw | Small | Small |

Table 1: GNSS stations classified by $|\Delta Z|$

| GNSS station | Geodetic coordinates | | | Classification | | |
| | Longitude [°] | Latitude [°] | Height [m] | K-G | ERA-Interim | MERRA-2 |
|---|---|---|---|---|---|---|
| BRAZ | -47.8779 | -15.9475 | 1106.0 | Aw | Large | Large |
| UBER | -48.3170 | -18.8895 | 791.8 | Aw | Small | Small |
| MARA | -71.6244 | 10.6740 | 28.4 | BSh | Large | Small |
| MERI | -89.6203 | 20.9800 | 7.9 | BSh | Small | Small |
| PEPE | -40.5061 | -9.3844 | 369.1 | BSh | Large | Small |
| MDO1 | -104.0150 | 30.6805 | 2004.5 | BSk | Critical | Critical |
| MZAC | -68.8756 | -32.8952 | 859.9 | BSk | Critical | Large |
| AREQ | -71.4928 | -16.4655 | 2488.9 | BWk | Large | Large |
| COPO | -70.3382 | -27.3845 | 479.1 | BWk | Critical | Critical |
| BRMU | -64.6963 | 32.3704 | -11.6 | Cfa | Small | Small |
| EBYP | -55.8922 | -27.3689 | 139.8 | Cfa | Small | Small |
| IGM1 | -58.4393 | -34.5722 | 50.7 | Cfa | Small | Small |
| ISPA | -109.3444 | -27.1250 | 112.5 | Cfa | Large | Large |
| LPGS | -57.9323 | -34.9067 | 29.9 | Cfa | Small | Small |
| POAL | -51.1198 | -30.0740 | 76.7 | Cfa | Small | Small |
| PPTE | -51.4085 | -22.1199 | 431.0 | Cfa | Small | Small |
| SMAR | -53.7166 | -29.7189 | 113.1 | Cfa | Small | Small |
| UFPR | -49.2310 | -25.4484 | 925.8 | Cfa | Large | Large |
| UNRO | -60.6284 | -32.9594 | 66.9 | Cfa | Small | Small |
| AZUL | -59.8813 | -36.7670 | 158.3 | Cfb | Small | Small |
| BOGT | -74.0809 | 4.6401 | 2576.4 | Cfb | Critical | Critical |
| CHPI | -44.9852 | -22.6871 | 617.4 | Cfb | Large | Large |
| POLI | -46.7303 | -23.5556 | 730.6 | Cfb | Small | Large |
| FALK | -57.8741 | -51.6937 | 50.8 | Cfc | Small | Small |
| PARC | -70.8799 | -53.1370 | 22.3 | Cfc | Large | Large |
| RIO2 | -67.7511 | -53.7855 | 32.0 | Cfc | Large | Small |
| CONZ | -73.0255 | -36.8438 | 180.6 | Csb | Small | Small |
| GUAT | -90.5202 | 14.5904 | 1519.9 | Csb | Large | Large |
| SANT | -70.6686 | -33.1503 | 723.1 | Csb | Critical | Critical |
| MGBH | -43.9249 | -19.9419 | 974.8 | Cwa | Small | Small |

Table 1: GNSS stations classified by $|\Delta Z|$

| | Geodetic coordinates | | | Classification | | |
|---|---|---|---|---|---|---|
| GNSS station | Longitude [°] | Latitude [°] | Height [m] | K-G | ERA-Interim | MERRA-2 |
| UCOR | -64.1935 | -31.4350 | 462.8 | Cwa | Large | Large |
| LPAZ | -110.3194 | 24.1388 | -6.9 | Cwb | Large | Large |
| UNSA | -65.4076 | -24.7275 | 1257.8 | Cwb | Critical | Critical |
| OHI2 | -57.9013 | -63.3211 | 32.5 | EF | Small | Large |
| PALM | -64.0511 | -64.7751 | 31.1 | EF | Large | Large |
| VESL | -2.8418 | -71.6738 | 862.4 | EF | Large | Large |
| AUTF | -68.3036 | -54.8395 | 71.9 | ET | Large | Large |

Table 2: Inter-annual mean of IWV ($\overline{IWV}^*$ in $[kg\ m^{-2}]$) for stations classified as Small, Large and Critical height difference. SD refers to the standard deviation. $\Delta Z$ [m.] refers to the difference between the geopotential height of the GNSS station and the bi-linear interpolated value of the geopotential height from each NWM.

| | | GNSS | | ERA-Interim | | | MERRA-2 | | |
|---|---|---|---|---|---|---|---|---|---|
| | Name | $\overline{IWV}^*$ | SD | $\Delta Z$ | $\overline{IWV}^*$ | SD | $\Delta Z$ | $\overline{IWV}^*$ | SD |
| **SMALL** | BELE | 49.65 | 7.09 | -39.88 | 49.25 | 6.83 | -32.44 | 51.55 | 7.21 |
| | RIOB | 46.87 | 8.46 | 11.29 | 47.71 | 7.98 | 16.34 | 49.34 | 8.35 |
| | SAVO | 35.66 | 8.53 | 20.88 | 36.09 | 8.19 | 34.72 | 36.23 | 8.83 |
| | MAPA | 49.99 | 6.92 | -60.84 | 49.65 | 6.79 | -47.28 | 51.17 | 7.16 |
| | POVE | 50.37 | 8.80 | 33.71 | 46.61 | 8.66 | 35.91 | 51.27 | 8.33 |
| | RNNA | 40.41 | 8.72 | -42.51 | 38.68 | 8.21 | -4.14 | 39.76 | 9.16 |
| | BOAV | 50.19 | 5.80 | -70.73 | 48.64 | 5.34 | -49.38 | 51.59 | 5.49 |
| | CHET | 42.06 | 10.66 | -37.16 | 41.43 | 10.17 | -28.66 | 42.45 | 10.89 |
| | CRO1 | 38.50 | 9.14 | -73.65 | 39.30 | 8.97 | -76.69 | 39.49 | 9.38 |
| | SALU | 47.86 | 7.07 | -25.31 | 47.32 | 6.85 | -21.79 | 48.92 | 7.63 |
| | TAMP | 36.64 | 11.90 | 5.49 | 37.28 | 11.61 | -17.99 | 36.62 | 11.89 |
| | VITH | 39.11 | 9.17 | -46.50 | 39.81 | 9.02 | -43.11 | 39.75 | 9.56 |
| | UBER | 27.74 | 11.00 | 40.34 | 29.94 | 10.82 | -14.81 | 30.32 | 11.41 |
| | MERI | 38.86 | 11.26 | -28.17 | 38.96 | 11.02 | -15.75 | 39.07 | 11.56 |
| | BRMU | 29.65 | 12.14 | -44.30 | 29.98 | 11.84 | -44.18 | 30.43 | 12.04 |
| | EBYP | 28.44 | 13.34 | 17.77 | 29.11 | 12.93 | 11.70 | 29.27 | 13.49 |
| | IGM1 | 19.77 | 10.01 | 48.58 | 20.64 | 10.25 | 53.37 | 20.59 | 10.22 |
| | LPGS | 19.31 | 9.78 | 31.74 | 19.91 | 9.83 | 33.51 | 20.03 | 9.90 |
| | POAL | 26.61 | 11.62 | -48.94 | 25.60 | 11.32 | 39.22 | 26.97 | 11.86 |
| | PPTE | 30.74 | 12.11 | 44.89 | 32.12 | 11.82 | 29.41 | 33.11 | 12.47 |
| | UNRO | 21.46 | 10.87 | 43.57 | 22.09 | 11.11 | 53.45 | 21.43 | 10.91 |
| | SMAR | 25.69 | 12.03 | -83.77 | 25.20 | 11.57 | -90.17 | 25.45 | 11.91 |
| | AZUL | 16.86 | 8.54 | 35.97 | 17.95 | 8.87 | 32.30 | 17.93 | 8.76 |
| | FALK | 10.98 | 4.50 | 57.56 | 11.41 | 4.56 | 46.53 | 11.70 | 4.60 |
| | CONZ | 14.15 | 5.84 | 33.72 | 13.95 | 5.51 | 84.21 | 14.38 | 5.92 |
| | MGBH | 26.55 | 10.10 | 70.90 | 27.54 | 9.76 | 16.00 | 28.48 | 10.32 |
| **LARGE** | ONRJ | 36.42 | 11.78 | -117.45 | 34.64 | 11.36 | -124.99 | 35.43 | 11.87 |
| | RIOD | 37.72 | 11.92 | -211.95 | 34.35 | 11.33 | -207.70 | 35.01 | 11.82 |

Table 2: Inter-annual mean of IWV ($\overline{IWV}^*$ in $[kg\ m^{-2}]$) for stations classified as Small, Large and Critical height difference. SD refers to the standard deviation. $\Delta Z$ [m.] refers to the difference between the geopotential height of the GNSS station and the bi-linear interpolated value of the geopotential height from each NWM.

| | | GNSS | | ERA-Interim | | | MERRA-2 | | |
| | Name | $\overline{IWV}^*$ | SD | $\Delta Z$ | $\overline{IWV}^*$ | SD | $\Delta Z$ | $\overline{IWV}^*$ | SD |
|---|---|---|---|---|---|---|---|---|---|
| | ACYA | 41.39 | 11.78 | -367.72 | 37.61 | 11.37 | -340.88 | 38.42 | 11.73 |
| | CEFE | 37.43 | 11.02 | -201.99 | 34.56 | 10.36 | -217.97 | 35.21 | 11.00 |
| | MANA | 44.85 | 9.90 | -113.84 | 42.40 | 10.09 | -101.02 | 43.74 | 10.72 |
| | MSCG | 31.68 | 11.10 | 241.03 | 34.52 | 11.33 | 173.53 | 34.64 | 12.09 |
| | PBCG | 33.68 | 7.90 | 165.08 | 33.38 | 7.52 | 147.99 | 33.98 | 8.47 |
| | SCUB | 37.83 | 10.29 | -138.75 | 37.88 | 10.03 | -164.51 | 37.73 | 10.40 |
| | SSIA | 36.53 | 8.69 | 181.75 | 39.89 | 9.01 | 178.23 | 41.80 | 9.69 |
| | BRAZ | 26.25 | 9.89 | 125.69 | 28.26 | 9.73 | 126.97 | 29.22 | 10.80 |
| | AREQ | 11.02 | 6.71 | -203.27 | 10.60 | 6.43 | -341.84 | 11.88 | 6.13 |
| | ISPA | 26.35 | 7.68 | 107.18 | 25.75 | 6.85 | 106.23 | 26.23 | 6.98 |
| | UFPR | 23.69 | 10.03 | 243.15 | 26.66 | 10.17 | 153.10 | 27.06 | 10.57 |
| | CHPI | 29.48 | 10.51 | -252.47 | 27.60 | 9.91 | -323.87 | 27.51 | 10.32 |
| | PARC[†] | 10.21 | 4.51 | -117.12 | 11.02 | 4.65 | -59.50 | 11.61 | 3.43 |
| | GUAT | 22.85 | 7.56 | 443.91 | 30.00 | 8.31 | 328.58 | 30.98 | 9.10 |
| | UCOR[†] | 18.51 | 9.98 | -145.30 | 19.44 | 9.56 | -94.83 | 18.57 | 9.22 |
| | LPAZ | 25.34 | 15.37 | -146.73 | 24.90 | 15.03 | -165.53 | 25.08 | 15.31 |
| | PALM | 6.81 | 3.16 | -132.37 | 6.34 | 2.77 | -165.08 | 6.53 | 2.86 |
| | VESL | 3.14 | 0.94 | 106.15 | 1.91 | 1.19 | 241.94 | 2.25 | 1.36 |
| | AUTF | 10.18 | 3.79 | -150.13 | 9.75 | 4.06 | -228.66 | 9.51 | 3.89 |
| CRITICAL | CUCU | 43.14 | 5.80 | -842.18 | 32.87 | 5.22 | -645.50 | 34.46 | 5.79 |
| | MDO1 | 10.20 | 7.64 | 688.88 | 15.42 | 10.13 | 630.23 | 15.34 | 10.36 |
| | COPO | 11.94 | 5.37 | -748.63 | 8.89 | 4.58 | -532.69 | 9.88 | 4.28 |
| | BOGT | 19.61 | 3.29 | 736.63 | 26.79 | 3.26 | 643.76 | 28.36 | 3.75 |
| | SANT | 12.52 | 5.09 | -1698.36 | 6.93 | 3.49 | -577.70 | 7.98 | 4.11 |
| | UNSA | 19.08 | 10.07 | -706.68 | 16.69 | 8.01 | -707.45 | 15.43 | 8.78 |

[†] Stations with $|\Delta Z|$ between GNSS and the four MERRA-2's grid points > 100 m.
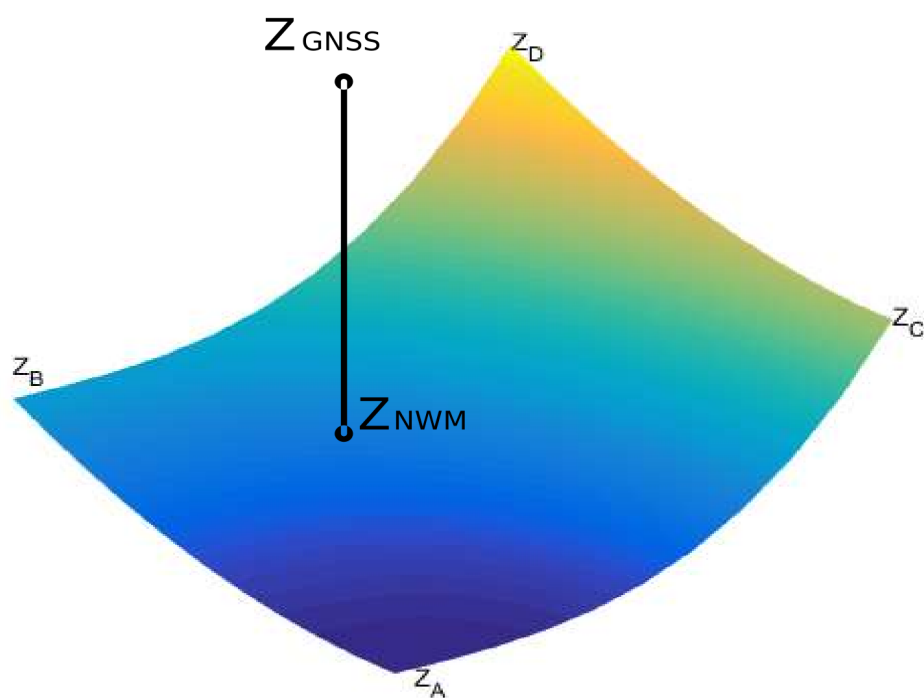
**Figure 1.** Example of geopotential height differences used to classify GNSS stations. $Z_{NWM}$ results from a bi-linear interpolation of the gridded data. A, B, C and D are the four grid points of the NWM around the GNSS station.
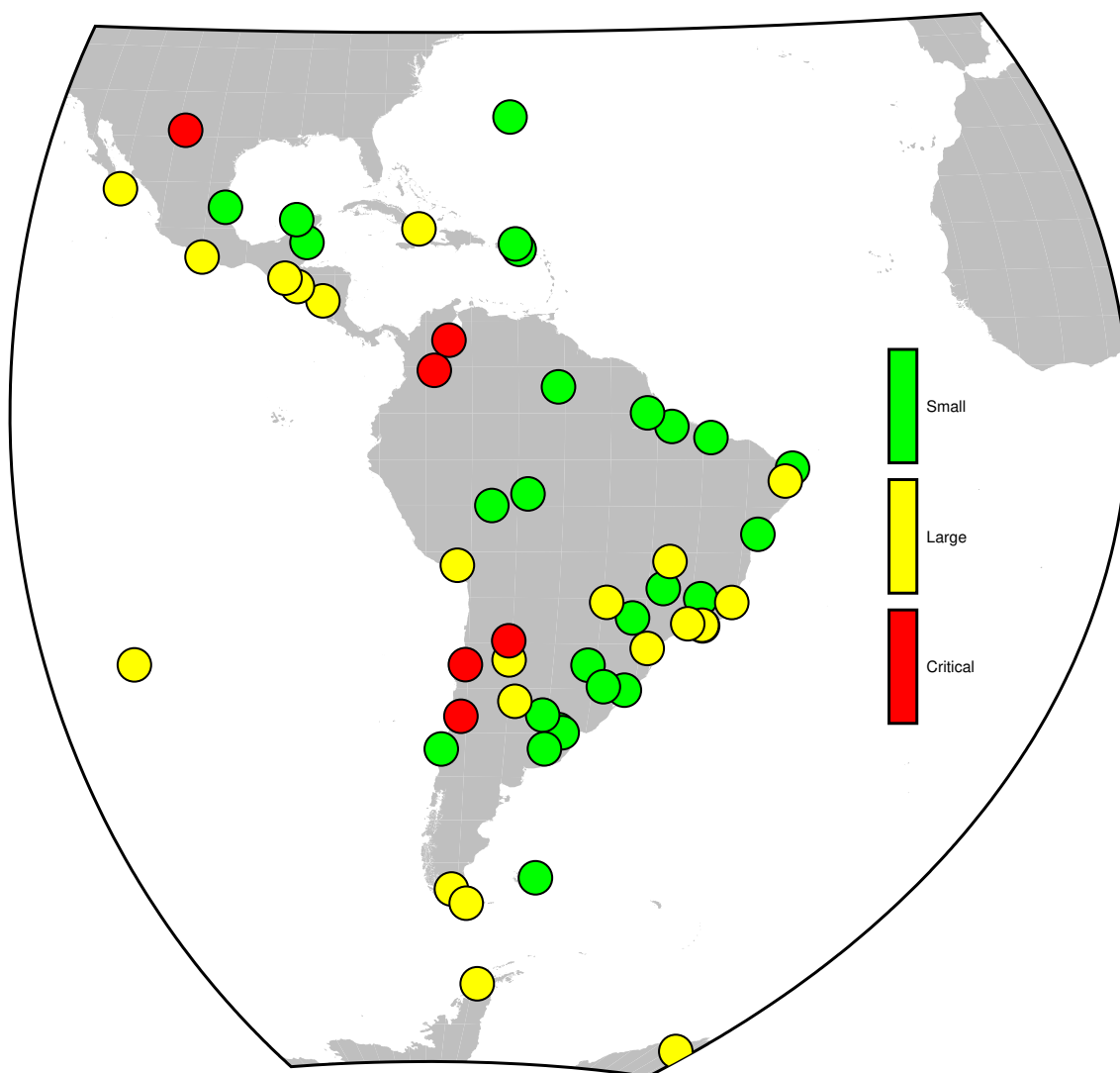
**Figure 2.** Station classification according to the difference between GNSS geopotential heights and the static geopotential heights from ERA-Interim ($Z_{GNSS} - Z_{ERA-Interim}$).
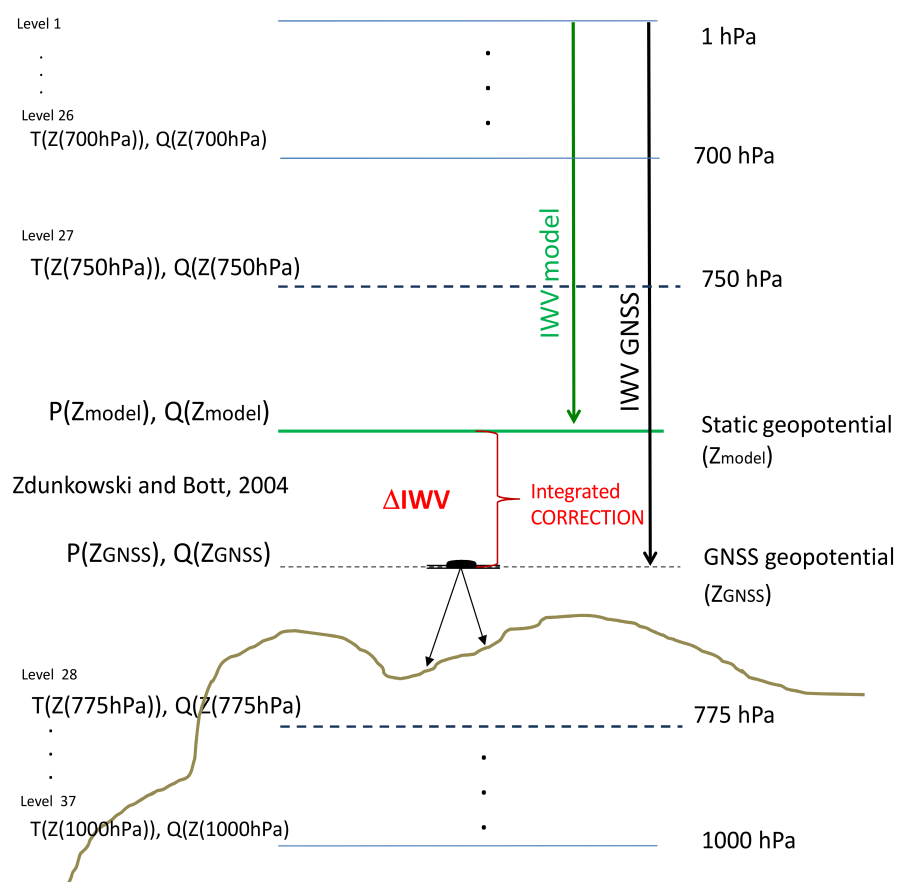
**Figure 3.** Scheme of the applied correction to the IWV from ERA-Interim reanalysis.
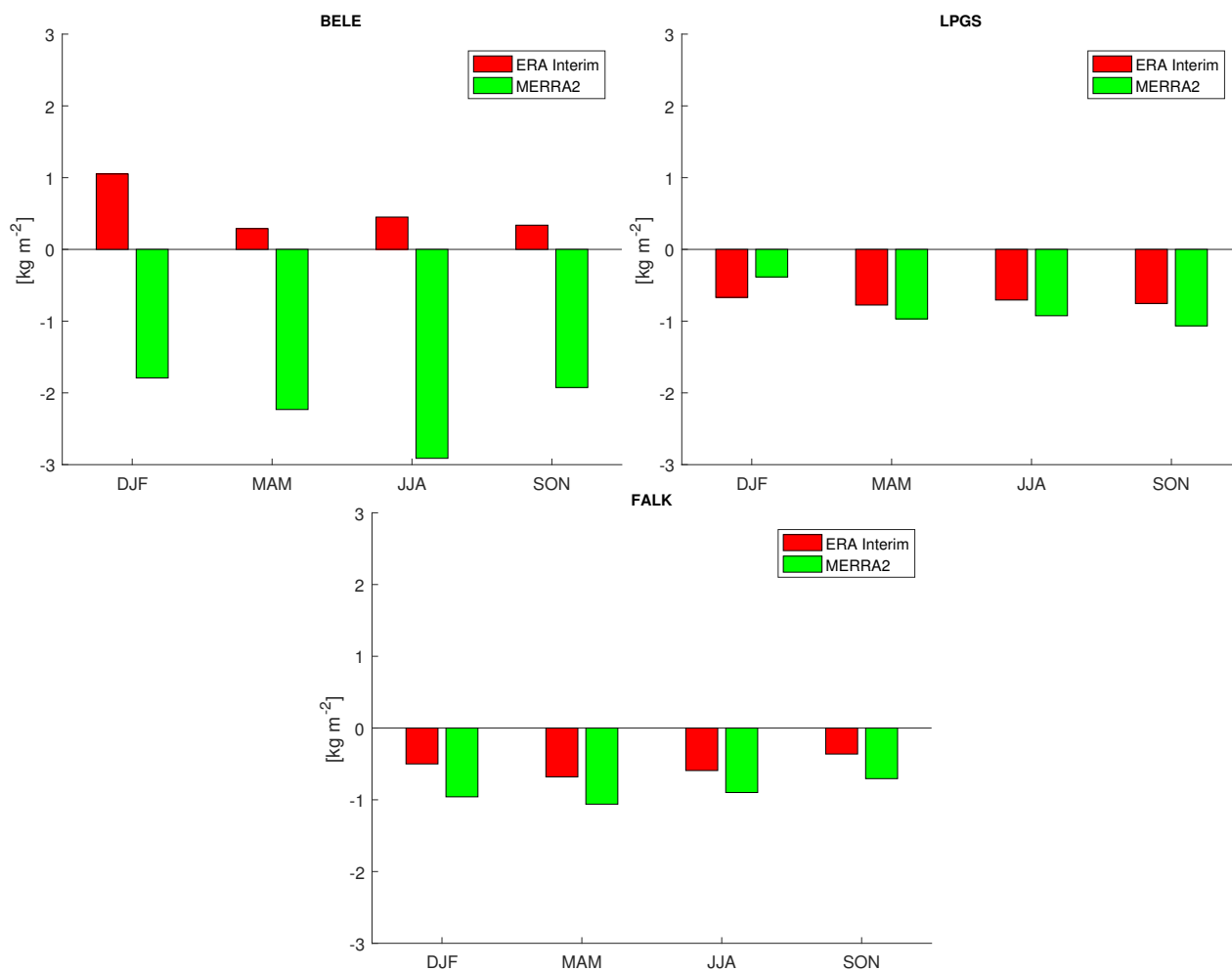
**Figure 4.** Differences of ($IWV_{GNSS} - IWV_{NWM}$) seasonally stacked for Small height difference stations. Both reanalysis models are shown: ERA-Interim in red and MERRA-2 in green. (from left to right and up to down) Examples for $\overline{IWV} > 30 \ kg \ m^{-2}$ (BELE), 12 $kg \ m^{-2} \leqslant \overline{IWV} \leqslant 30 \ kg \ m^{-2}$ (LPGS) and $\overline{IWV} < 12 \ kg \ m^{-2}$ (FALK)
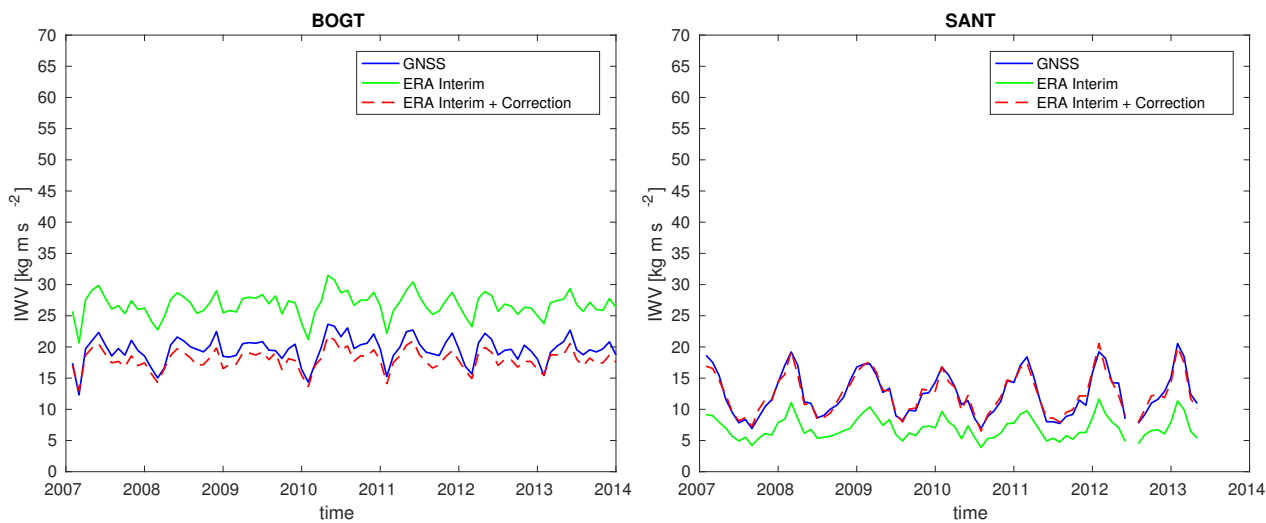
**Figure 5.** GNSS IWV (blue, solid line) and ERA-Interim IWV (green, solid line) data time series for 2 critical stations shown as an example: BOGT in Bogotá, Colombia ( $\Delta Z$ = 736 m.) and SANT in Santiago de Chile, Chile ( $\Delta Z$ = -1037 m.). The IWV values as a result of the addition of the computed correction plus IWV values from ERA-Interim are also shown (red, dashed line)
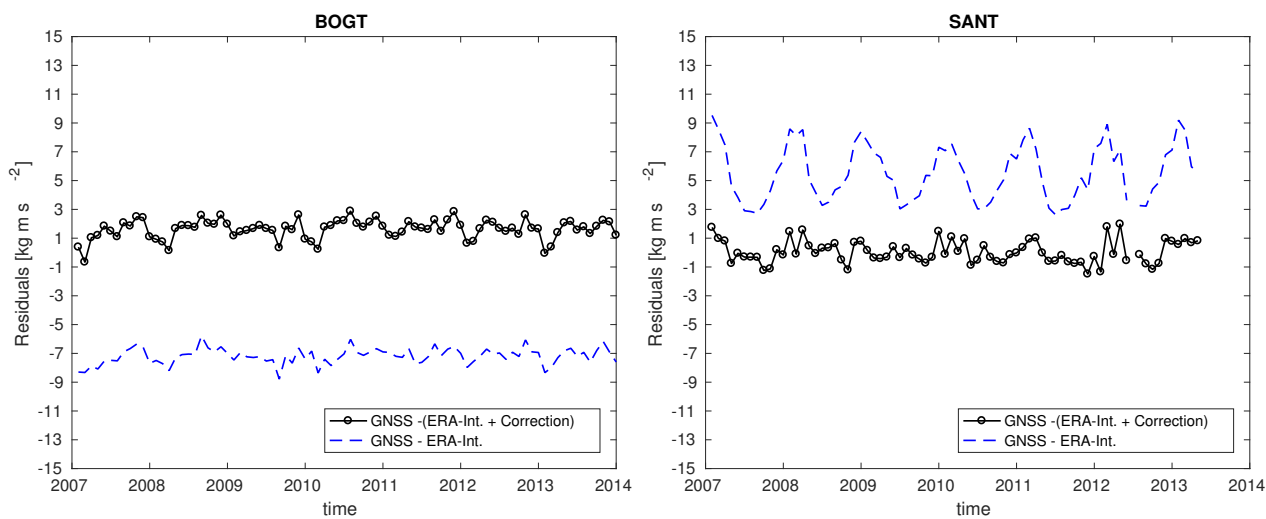
**Figure 6.** Residuals of the difference $(IWV_{GNSS} - IWV_{ERA-Interim})$ (blue, dashed line) along with residuals of the difference $[IWV_{GNSS} - (IWV_{ERA-Interim} + correction)]$ (solid black line)
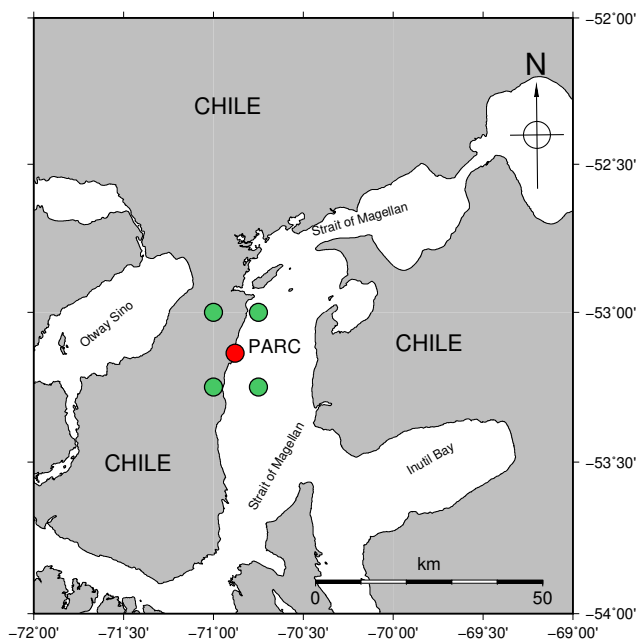
**Figure 7.** Location of GNSS station PARC along with the 4 grid points around the station. The grid points correspond to ERA-Interim.